Article

Damage Evolution Characteristics and Constitutive Model for Coal and Rock under Asymmetric Loading

Tao Wang, Hongbao Zhao, Xiangyang Zhang,* Wenpu Li, and Shuangli Du

Cite This: *ACS Omega* 2024, 9, 16687−16700

Read Online

ACCESS | Metrics & More | Article Recommendations

ABSTRACT: Tunnels and shaft mining roadways are often subjected to varying degrees of asymmetric loading due to terrain relief or project excavation. In order to analyze the influence of the asymmetric degree of loading on the mechanical properties and damage rupture law of coal rock, uniaxial compression tests of coal rock under four asymmetric loading modes were carried out, the influence of the asymmetric coefficients of loading on macro- and micromechanical properties of coal and rock was analyzed, and a statistical damage constitutive model of coal and rock was established to reflect the asymmetric loading degree. The results of the study show that the peak stress of the coal rock decreases gradually with the increase in the asymmetric coefficient of loading, and the two are linear functions of each other. The distribution of the acoustic emission ringing count peak value is concentrated under uniform loading, while the acoustic emission ringing count rate presents a multipeak phenomenon under asymmetric loading, and the peak value points are scattered. In the case of asymmetric loading, the stress concentration on the edge of the upper loading plate leads to shear failure, and the microscopic cracks are concentrated near the interface between the loading zone and the nonloading zone. According to the established damage constitutive model, when the damage degree is the same, the larger the asymmetric coefficient, the smaller the strain value, which indicates that the asymmetric loading promotes the damage of coal and rock.
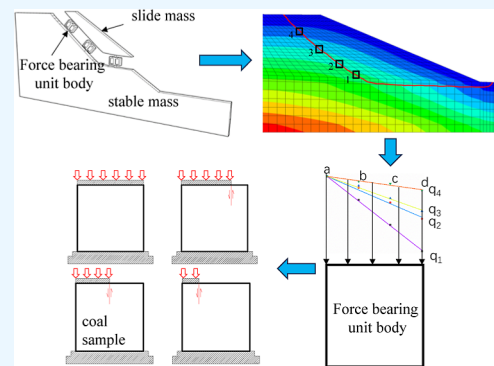
1. INTRODUCTION

The problem of stress-induced rock deformation and damage is a frequently encountered problem in geotechnical and mining engineering.[1−3] Under some special working conditions, rocks will experience deformation and damage processes under asymmetric loading environments due to the influence of the host environment or mining disturbances.[4,5] For example, due to the undulation of the overlying mountains of the tunnel, the rock mass around the tunnel excavation is subjected to asymmetric loading, as shown in Figure 1a. At the same time, the existence of protective coal pillars left behind by the upper coal mining also leads to an asymmetric loading effect on the working face transportation roadway during the lower coal mining, as shown in Figure 1b. Therefore, the study of the deformation behavior and the crack extension behavior of rock bodies under asymmetric loading is particularly important for understanding the fracture mechanism of rock bodies and predicting geo-hazards in rock engineering.

The coal body shows different mechanical properties under different stress modes. Zhao et al. found that the uniaxial compressive strength and longitudinal wave velocity of coal are affected by the degree of angle between the loading direction and the bedding plane.[6] Xin et al. compared and analyzed the differences of mechanical properties and permeability of coal under conventional triaxial compression, phased variable speed triaxial compression, unloading confining pressure (UCP), and

phased variable speed UCP (PVSUCP).[7] Liu et al. found that the mechanism for unloading-induced coal strength reduction comes from the confining pressure unloading-induced increase in shear stress on the fracture surface and a decrease in shear strength.[8] Ding et al. used the RMT-150B rock mechanics test system to perform uniaxial compression and uniaxial cyclic loading−unloading tests with different stress levels and found that cyclic loading exhibits a clear enhancement effect on the strength of coal masses, and the failure mode of coal samples is more severe.[9] The evolution of the strength, surface deformation, crack propagation, and elastic strain energy of coal under various loading rates was investigated by Gao et al.[10]

Coal rock destabilization damage is a dynamic evolution process in which its internal cracks continuously start to crack and expand until penetration. Acoustic emission monitoring technology is considered to be an effective method to study the damage and destruction process of coal rock and to characterize the destruction mechanism of coal rock.[11] Shan et al.
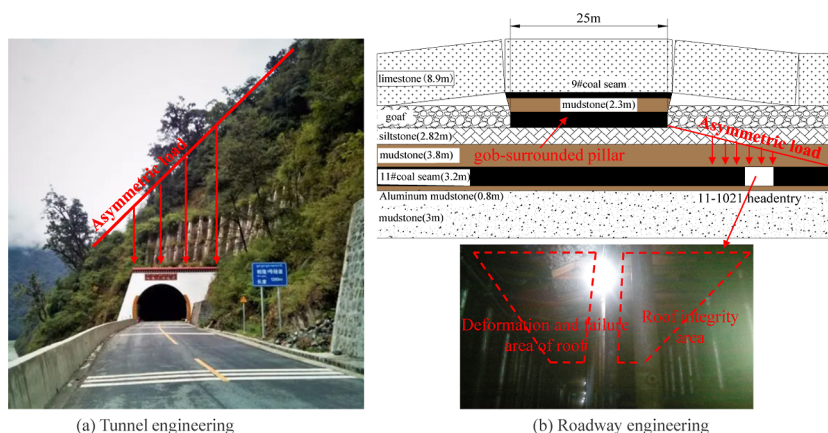
(a) Tunnel engineering   (b) Roadway engineering
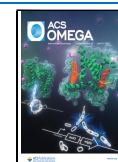
Figure 1. Problems of asymmetric loading in geotechnical engineering. (a) Tunnel engineering and (b) roadway engineering.

investigated the effect of water content on the damage characteristics of loaded coal rock with the help of acoustic emission technology.[12] Cui et al. elucidated the relationship between strain and damage variables during uniaxial compression by analyzing the acoustic emission ringing number.[13] Through the improved G−P algorithm, Gu calculated the fractal characteristics of acoustic emission parameters and concluded that the sudden decrease of fractal dimension could be used as a criterion for the damage precursor of coal samples.[14] With the development of computers, numerical simulation technology has shown unique advantages in the study of the evolutionary characteristics of coal rock microfracture emergence and expansion.[15] Liu used the PFC program to establish coal rock assemblage specimens with different height ratios and analyzed the effect of height ratio on the mesomechanical properties of the assemblage specimens.[16] Wu et al. investigated the mesodamage and energy evolution of coal samples containing holes during uniaxial compression using the PFC program and concluded that the holes had a significant effect on the crack initiation stress and energy characteristics in the prepeak stage.[17] In order to analyze the influence of crack inclination angle on the mechanical properties of coal samples, Liu established a two-dimensional numerical model of coal samples with different crack inclination angles by using the particle flow program and carried out a simulation of the damage evolution process of coal samples under uniaxial compression conditions.[18]

The establishment of a damage model of rock is of great significance for analyzing and predicting the deformation characteristics of rock engineering materials, and how to establish the quantitative relationship between the parameters obtained from the test and the mechanical parameters and predict the destabilizing damage of the rock body is still a hot spot and a difficult point in the research of rock mechanics. Sun et al. used digital image processing techniques to determine the quantitative information on mesocracks in coal samples and established an elastic-brittle damage model based on meso-structural information on coal bodies.[19] Huang adopted a graded loading creep test method to study the creep characteristics of coal samples under different initial damage conditions and improved the creep model in the acceleration stage by establishing the relationship between damage variables and initial damage.[20] Xu et al. carried out a uniaxial compression mechanical characterization of coal samples with different water contents, introduced the damage variable based on energy dissipation, and proposed to consider the effect of submergence time.[21]

Scholars from various countries have carried out a large number of studies on the mechanical properties and damage breakage laws of coal rocks and have achieved fruitful research results. However, most of the existing research results are based on homogeneous loading conditions such as conventional uniaxial compression or triaxial compression, and research on the deformation and damage law of coal rock under asymmetric loading is rarely reported. Zang et al. investigated the mechanical properties and damage rupture law of rocks under uniaxial compression and triaxial compression with asymmetric loading but did not consider the effect of different asymmetric coefficients on the damage evolution law of rocks.[22,23] Wang et al. carried out a study on the damage and failure law of large size rock-like materials under nonuniformly distributed loading and proposed the regionalized characteristics of rock damage and failure.[24] Wang et al. studied the mechanical properties and damage law of coal rock under different asymmetric coefficients with the help of the digital speckle method but lacked the study of the influence of the change in asymmetric load coefficients on the damage process of coal rock from a mesoscopic perspective.[25]

Therefore, with the help of the acoustic emission and particle discrete element program, this paper investigated the influence law of asymmetric coefficients on the damage and rupture of coal rock from the macro- and mesoperspectives, revealed the mechanism of damage and rupture of coal rock caused by asymmetric load, and established the damage ontological model considering the influence of asymmetric load. The research results of the thesis can provide a theoretical basis for the determination of the width of coal pillars for end-help coal mining in open pit coal mines under the condition of eccentric loading as well as the interpretation of deformation and instability of the roadway.

2. EXPERIMENTAL AND NUMERICAL DETAILS

2.1. Coal Sample Preparation. The specimens used in the indoor tests were cut and polished from raw coal briquettes. The bulk of the raw coal is taken from the Ganhe Mine of the Huozhou Coal and Electricity Group in Shanxi Province. The processing of coal samples was carried out in strict accordance with the standards recommended by the American Society for Testing and Materials, and the size of the prepared raw coal specimens was 70 × 70 × 70 mm. In order to minimize the influence of primary fissures on the mechanical properties of the coal samples, ultrasonic testing methods were used to screen the

raw coal samples so that the differences in the wave velocity values of the samples were less than 100 m/s. The prepared raw coal samples and the ultrasonic testing equipment are shown in Figure 2.

(a) raw coal sample   (b) supersonic reflectoscope
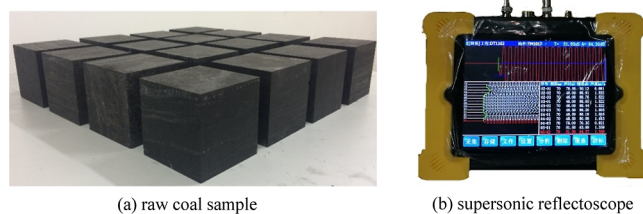
Figure 2. Raw coal sample and ultrasonic detection device. (a) Raw coal sample and (b) supersonic reflectoscope.

2.2. Testing System and Loading Procedure. The loading system is a TAW-3000 microcomputer-controlled electro-hydraulic servo rock three-axis testing machine, which has a variety of loading modes and has the advantages of high precision, high stability, and high sensitivity of the equipment. A PCI-II acoustic emission monitoring system was used to acquire coal rock acoustic emission signals during the loading process. The acoustic emission threshold was set to 45 dB, the pregain was set to 40 dB, the frequency range was set to 1 kHz to 1 MHz, the sampling frequency was 1000 ksamples/s, and the pretrigger was 256.

A total of 12 pieces of raw coal specimens were used in this test, which were divided into 3 groups of 4 specimens each to carry out uniaxial compression tests with loading areas of S, $0.75S$, $0.5S$, and $0.25S$ (S is the surface area of the coal sample, $S = 4900$ mm^2). Different degrees of asymmetric load application were realized by changing the position of the rigid pads, and the loading direction was perpendicular to the coal bedding direction in order to reduce the influence of the lamination effect on the mechanical and acoustic emission characteristics of the coal rock. The loading diagram is shown in Figure 3.

In order to achieve damage localization during coal rock loading, a total of 8 acoustic emission sensors were deployed in each coal sample, 2 on each side, located on the centerline of the side and 15 mm from the top and bottom edges of the coal sample, respectively. To increase the coupling effect between the acoustic emission transducer and the surface of the coal sample, a rubber band was used to fix the transducer to the surface of the coal sample, and petroleum jelly was applied between the transducer and the coal sample. In addition, petroleum jelly was applied between the rigid pads and the coal samples to minimize the effect of the end friction effect on the acoustic emission signals. The press was used in a displacement loading mode with a loading rate of 0.1 mm/min. Figure 4 shows the Taw-3000

servo-controlled test system and PCI-II Acoustic Emission system.

(a) Testing system   (b) Coal specimen with eight AE sensors
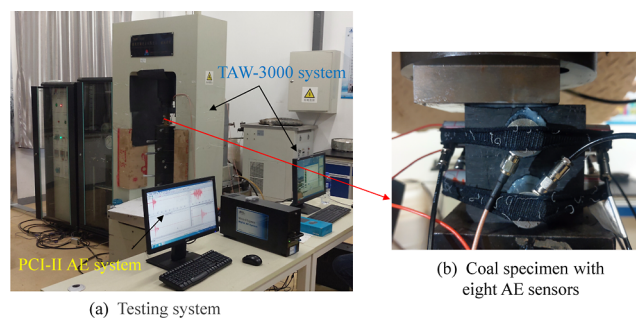
Figure 4. Taw-3000 servo-controlled test system and PCI-II acoustic emission system. (a) Testing system and (b) coal specimen with eight acoustic emission sensors.

2.3. Numerical Model and Microparameters. With the advantage of discrete elements in discontinuous problems such as cracking and separation of media, this paper adopts PFC2D software to study the damage rupture process of coal rock under asymmetric loading from a mesoscopic point of view.[26,27] The parallel bond model in PFC can withstand tensile stress and resist the relative rotation of particles. When the connection is broken, the parallel bond model degenerates into a linear contact model, and the particles will slide relative to each other under the tangential force, which is more suitable for the simulation of the damage rupture process of brittle materials such as rocks. Therefore, in this article, the parallel bonding model is used to explore the macroscopic and mesoscopic mechanical properties of coal rock under asymmetric loading.

A numerical simulation specimen with the same dimensions as the indoor test was built with a specimen size of 70×70 mm, which produced a total of 12,146 particles containing 23,771 contacts. The particle size obeyed a uniform distribution with a minimum particle radius of 0.25 mm and a particle size ratio of 1.66. The displacement loading mode is adopted to realize the loading of the specimen through the relative movement of the upper and lower walls, and the moving speed of the wall is set at 0.05 m/s to meet the requirements of quasi-static loading.[28] Determination of mesomechanical parameters is a prerequisite for numerical simulation using the discrete element method. Based on the macromechanical parameters and damage modes of coal rock obtained from indoor tests, this paper adopts the "trial and error method" to determine the fine mechanical parameters of coal rock specimens.[29] Table 1 shows the successfully calibrated mesomechanical parameters of the coal rock that can be used for subsequent simulations, and Figure 5 shows the comparative results of the stress−strain and

(a) λ=0   (b) λ=0.25   (b) λ=0.5   (b) λ=0.75
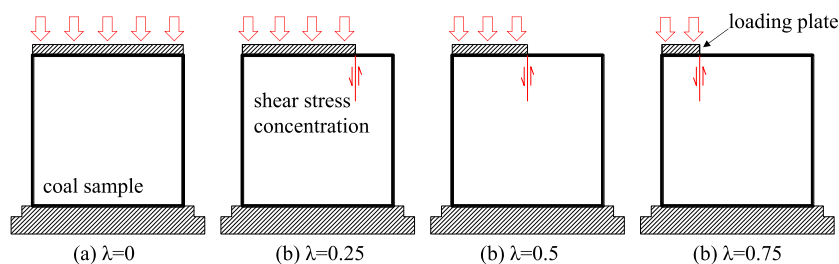
Figure 3. Schematic diagram of sample loading mode. (a) $\lambda = 0$, (b) $\lambda = 0.25$, (c) $\lambda = 0.5$, (d) $\lambda = 0.75$.

Table 1. Micromechanical Parameters of PFC2D for Coal Specimen in This Research

mesoscopic parameters	value
minimum particle radius, R_{min}/mm	0.25
ratio of radius, $R_{rat} = R_{max}/R_{min}$	1.66
friction coefficient between particles, μ	0.3
particle density, ρ/(kg/m³)	2500
elastic modulus between particles, E_c/GPa	1.5
contact bonding stiffness ratio, k_n/k_s	2.82
parallel bonding contact modulus, $\bar{E}_c$/GPa	1.5
parallel bonding cohesion, pb_coh/MPa	33
standard deviation of parallel bond cohesion/MPa	2
parallel bonding tensile strength, pb_ten/MPa	27
standard deviation of parallel bond tensile strength, MPa	2

Table 2. Comparison of Laboratory Test and Numerical Simulation Results

mechanical properties	experimental result	numerical result	deviation (%)
UCS/MPa	39.5	38.77	1.85
E/GPa	1.844	1.813	3.77

macroscopic damage modes of the coal rock obtained from the indoor tests and numerical simulations. Table 2 shows the mechanical parameters of coal rock obtained from indoor tests and numerical simulation.

As can be seen from Figure 5, the stress−strain curves of the coal rock obtained from the indoor tests are in good agreement with those obtained from the numerical simulation. The original coal specimen has a primary pore and fissure structure, the stress−strain curve has an initial compression-density stage, and the curve is up-concave. The numerical model particles are uniformly distributed and dense, and the stress−strain curve does not have a compression-density stage. As shown in Table 2, the peak uniaxial compression strength of raw coal obtained from the indoor test is 39.50 MPa, and the modulus of elasticity is 1.884 GPa. The peak uniaxial compression strength of raw coal obtained from the numerical simulation is 38.77 MPa, and the modulus of elasticity is 1.813 GPa. Comparison of the indoor test and the numerical simulation shows that there is a deviation of 1.85% in the peak strength and a deviation of 3.77% in the modulus of elasticity. From Figure 5b, it can be seen that the numerical simulations of uniaxial compression coal rock microscopic cracks are mainly tensile damage cracks, and the macroscopic damage mode is nearly X-type shear damage, which is caused by the microscopic tensile cracks of the macroscopic shear damage. Figure 5c shows the shape of the residual lumps after uniaxial compression damage of the coal sample, and it can be judged from the morphology of the residual lumps that the macroscopic damage mode of the original coal specimen under

the uniaxial compression condition is nearly X-type shear damage. In summary, the mechanical parameters and macroscopic damage modes obtained from the numerical simulation are in good agreement with the indoor test results, and the fine-scale parameters obtained from the calibration can be used in the subsequent numerical simulation study.

3. RESULTS AND DISCUSSION

3.1. Effect of the Degree of Loading Asymmetry on the Mechanical Parameters of Coal Rocks.

In uniaxial compression, the ratio of the load to the stressed area is used to characterize the stress of the specimen, and when asymmetric loading is applied, the calculation of the stress in the coal rock adopts the calculation of the equivalent stress, which is calculated according to eq 1.

$$\sigma_i = \frac{2\sigma_c}{1 + i/4} \tag{1}$$

where σ_c is the peak stress of coal rock under uniaxial compression condition, and σ_i is the equivalent stress of coal rock at different loading areas. Where $i = 1-4$ represent the equivalent stresses of coal rock when the asymmetric coefficient (ratio of unloaded area to total area of loaded surface) $\lambda = 0.75$, 0.5, 0.25, and 0, respectively.

Figure 6 shows the relationship between the peak stress and the asymmetric coefficient of coal rock obtained from the indoor test and numerical simulation. The average value of the peak stress obtained from the same loading conditions in the indoor tests was calculated, and the average of the indoor test peak stresses as well as the numerically simulated peak stresses were fitted to the relationship with the asymmetry factor, respectively; the results are shown in Figure 6.

As can be seen from Figure 6, with the increase of load asymmetry coefficient, the peak stress of coal rock decreases gradually, which is mainly because the increase of asymmetry coefficient makes the effective bearing area of coal rock decrease,

(a) Axial stress-strain curve   (b) Numerical result   (c) Experimental result
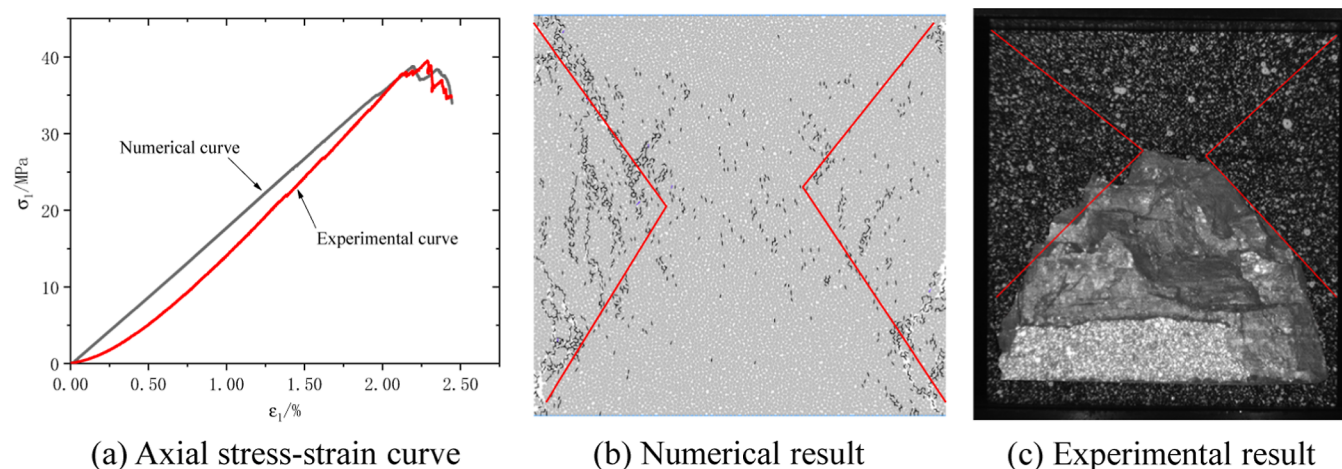
Figure 5. Comparison of indoor test and numerical simulation results. (a) Axial stress−strain curve, (b) numerical result, and (c) experimental result.
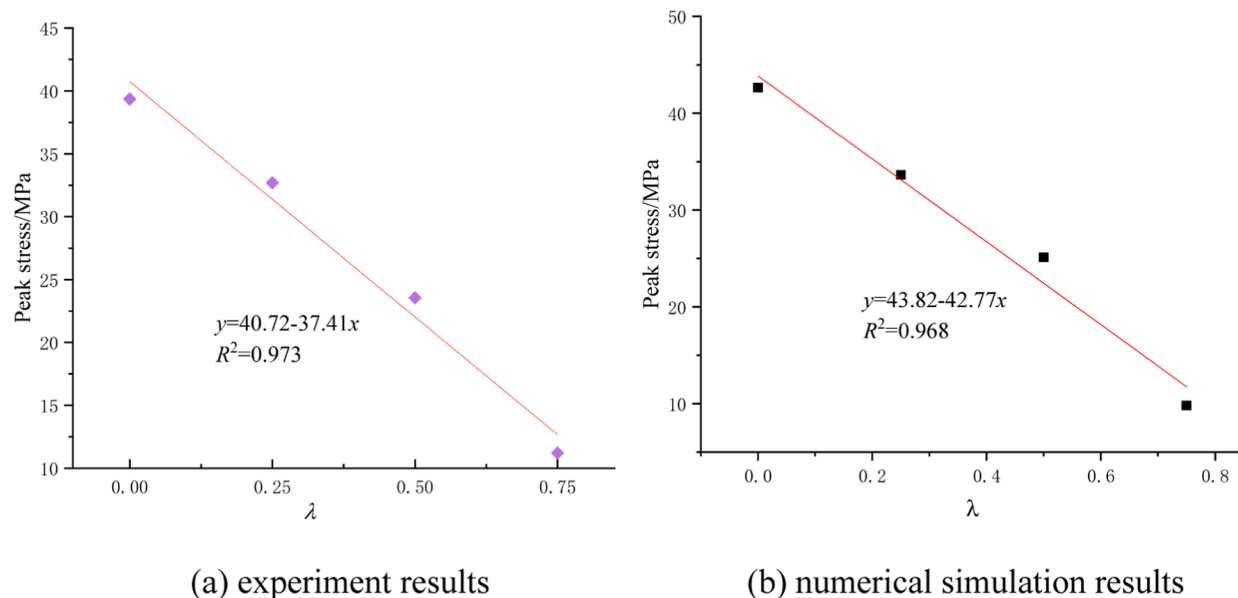
(a) experiment results   (b) numerical simulation results

Figure 6. Relationship between peak stress and asymmetric coefficient of coal. (a) Experimental results and (b) numerical simulation results.

(a) $\lambda=0$ (b) $\lambda=0.25$
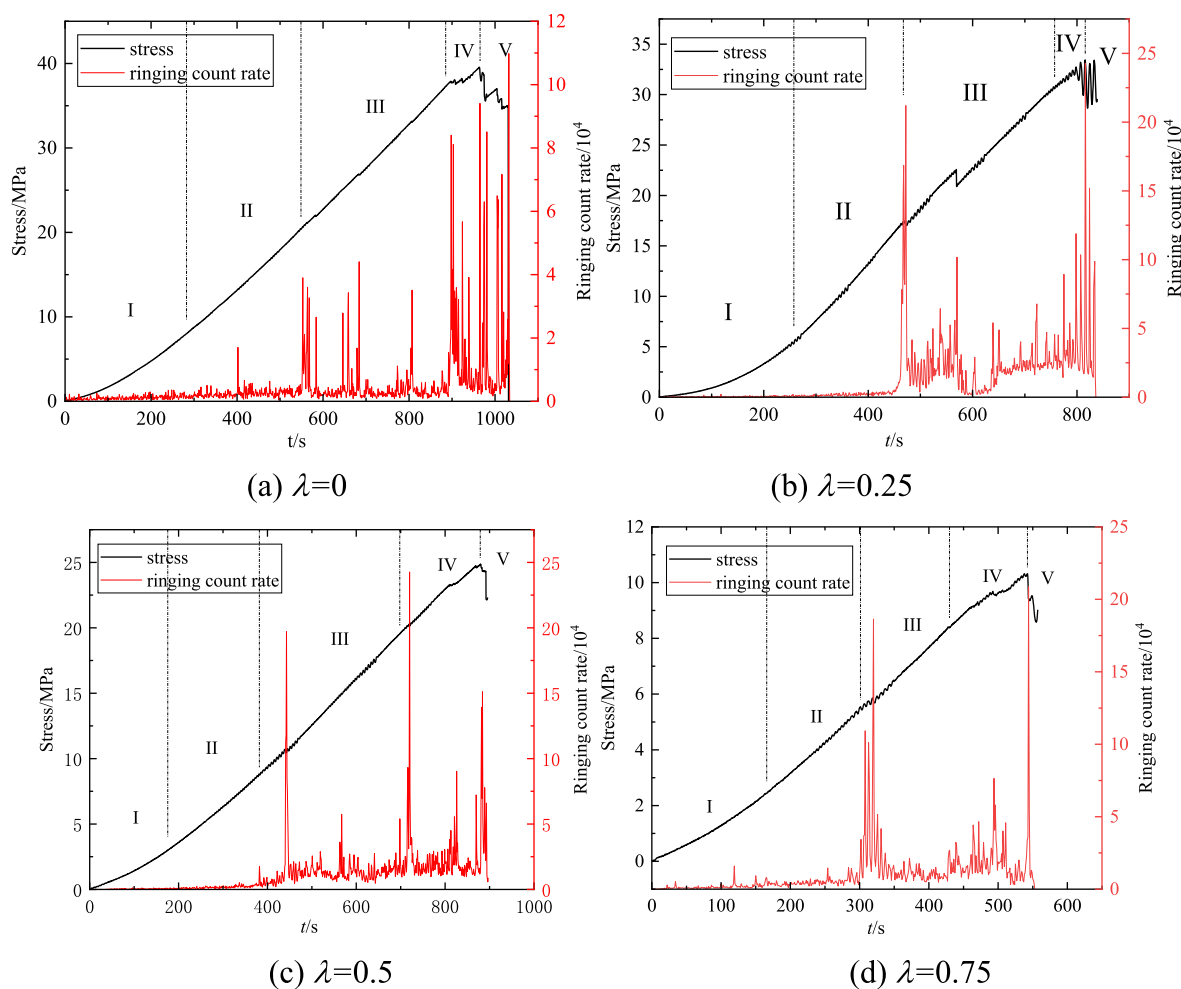
(c) $\lambda=0.5$ (d) $\lambda=0.75$

Figure 7. Changes of ring count rate with time (a) $\lambda = 0$, (b) $\lambda = 0.25$, (c) $\lambda = 0.5$, and (d) $\lambda = 0.75$.

and the degree of load eccentricity increases, making it more prone to damage of coal rock. Based on the data fitting, it was found that the peak coal rock stress from both indoor tests and

numerical simulations decayed with a linear function law as the asymmetric coefficient of loading increased.

3.2. Effect of the Degree of Load Asymmetry on the Acoustic Emission Parameters. The analysis of the acoustic

(a) λ=0

(b) λ=0.25

(c) λ=0.50

(d) λ=0.75
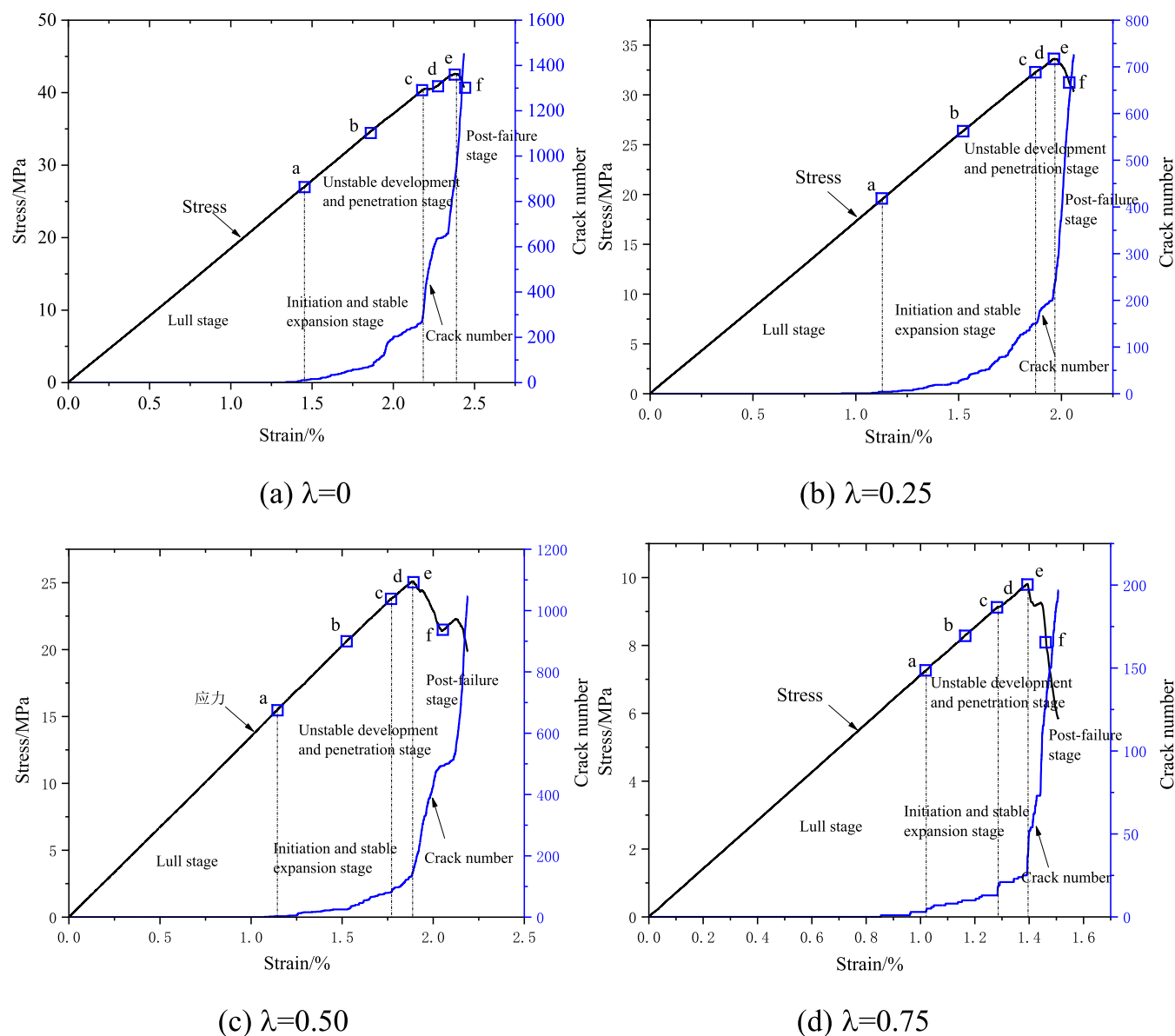
Figure 8. Evolution of the number of microcracks in samples with different asymmetric coefficients.

emission characteristics can obtain the evolution law of coal damage and crack extension.[24,30−32] The emission signals recorded in the indoor test were processed to obtain the acoustic emission ringing count rate at different loading moments. Figure 7 shows the evolution of the acoustic emission ringing count rate at different loading moments.

As can be seen from Figure 7, the variation of the acoustic emission parameters with time during both conventional uniaxial compression and asymmetric load compression of coal samples can be categorized into five stages. Initial compaction stage I: the stress curve of coal samples is concave at the early stage of loading, and the original micropores and microfissures in the coal samples are gradually closed under pressure; the number of acoustic ringing counts and the number of impacts in the coal samples under different loading areas are very few, and the released energy is close to zero. The reason for the small amount of acoustic emission signals at this stage is the occlusion damage and friction of the rough surface during the process of microfissure closure. Elastic deformation stage II: the stress−time curve of coal rock in the elastic stage is

approximately a straight line; the stress size is not enough to produce new cracks at this stage; the acoustic emission ringing count rate and the impact rate are very small and smooth; the energy rate is close to zero; and the energy is mainly stored in the form of elastic energy in the coal samples. The small amount of acoustic emission signals is mainly due to slippage of the coal sample at pre-existing fissures or a small amount of matrix deformation due to internal pore pressure resisting external pressure. Crack initiation and stable propagation stage III: during this stage, there are significant fluctuations in the acoustic emission ringing counting rate and impact rate. With the fluctuation of the ringing counting rate, the acoustic emission energy also showed corresponding fluctuations, indicating that new cracks gradually initiated and expanded during this stage, accompanied by the continuous release of energy. Under different loading areas, most of the specimens at the end of this stage will have a short period of plastic deformation with a small increase in stress and a significant increase in strain, in which the acoustic emission signal changes are more obvious. Unlike conventional uniaxial compression, the coal samples under

Figure 9. Surface crack distribution characteristics of samples at different loading times. (a) $\lambda = 0$, (b) $\lambda = 0.25$, (c) $\lambda = 0.5$, and (d) $\lambda = 0.75$.

asymmetric loading have a sudden change in the acoustic emission signal at the beginning of the stage, and the acoustic emission signal has an overall high and low level, with a large difference and a multipeak phenomenon. Crack instability development and penetration stage IV: in this stage, the acoustic emission ring count rate and impact rate increase dramatically and change drastically, and the acoustic emission energy rate reaches its maximum value at the peak stress moment. Dramatic changes in acoustic emission parameters are caused by crack expansion, in which a large number of cracks in the coal samples accelerate the expansion of the primary fissure penetration and continue to expand to form a network of fissures, which in turn develop into a macroscopic master-controlled penetrating fissure, and the specimen is destroyed. The peak acoustic emission signals of conventional uniaxial compression coal samples are more intensive in this stage, showing a multipeak phenomenon, while the coal samples under asymmetric loading show a single-peak phenomenon of acoustic emission signals in this stage. Postdamage stage V: there is a step-down phenomenon in the postdamage stress curves of coal samples under conventional uniaxial compression conditions, and the ringing count rate of acoustic emission maintains a high value with the impact rate, but the energy rate value is small, and this phenomenon may be caused by the mutual misalignment of macroscopic cracks. When asymmetric loading was applied, the main control cracks located in the loaded and unloaded areas rapidly penetrated when the coal samples reached the peak

stress, and most of the postpeak stress values fell rapidly, and the values of the acoustic emission parameters also decreased rapidly.

As can be seen from Figure 7, the asymmetric coefficient has a certain influence on the change rule of the coal rock acoustic emission parameters. At $\lambda = 0$, the acoustic emission ringing count peaks are more concentrated, mainly in the unstable crack development and penetration stage and the postdamage stage. When asymmetric loading is applied, the acoustic emission ring counts of the coal rock show high and low levels, and the difference is large. The acoustic emission ringing count rate shows the phenomenon of multiple peaks, and the peak points are more dispersed. These characteristics are found in the stable crack expansion stage, unstable crack development, and penetration stage. When the load is uniformly distributed, the coal sample is uniformly loaded, and the internal particles of the coal sample are extruded, slipped, and experience friction under the action of the uniform load, which generates a small amount of acoustic emission signals. As the load continues to increase, microcracks are generated at weak locations within the coal sample, which are generated at multiple locations within the coal sample; however, the microcracks at each location do not penetrate quickly, and the acoustic emission ringing count rate is relatively smooth. With further increase in loading, the microcracks forming the master cracks penetrate each other, and the acoustic emission ringing count rate increases rapidly to the peak point. With asymmetric loading, there is a stress
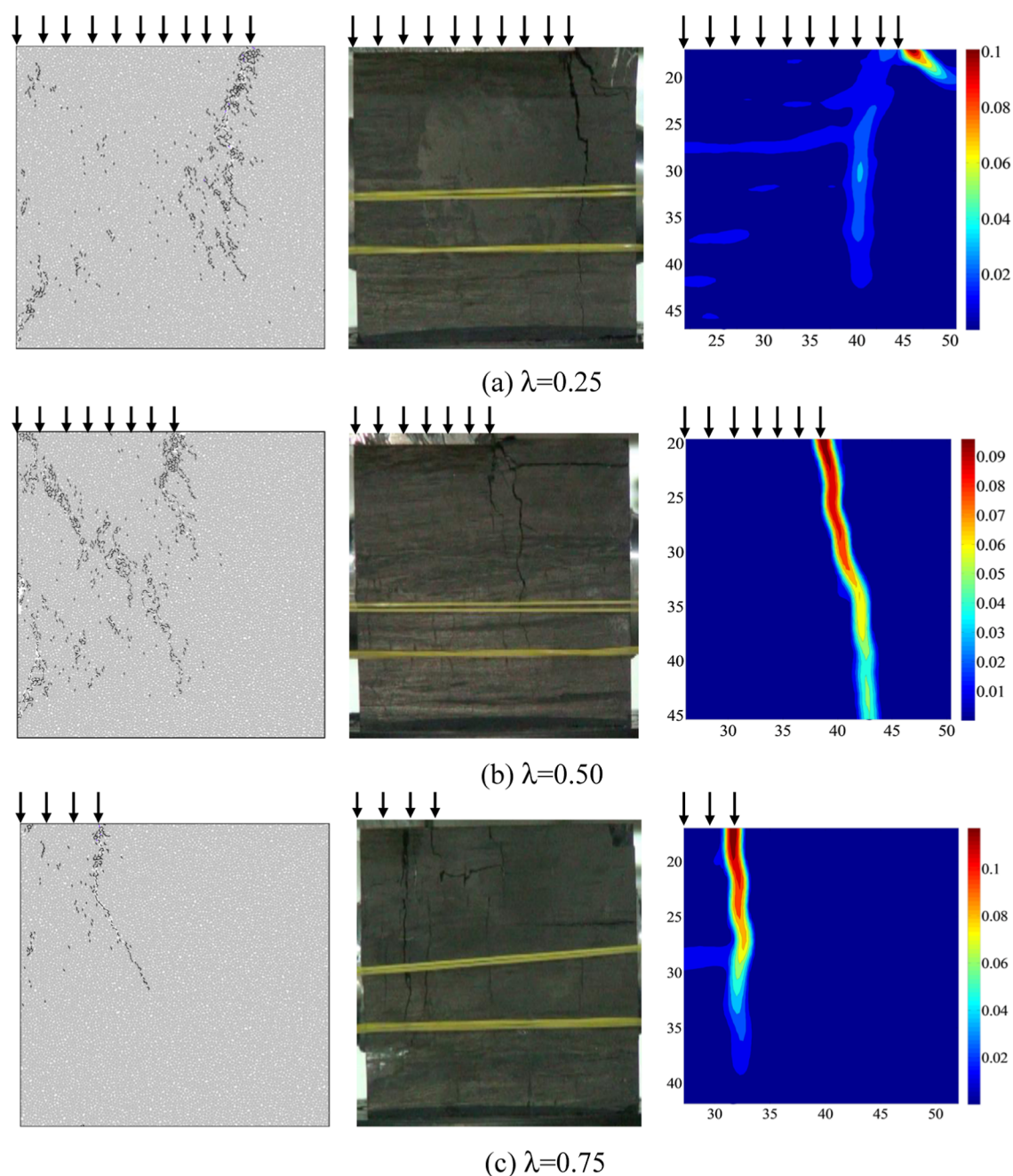
Figure 10. Comparison between the numerical and experimental failure modes. (a) $\lambda = 0.25$, (b) $\lambda = 0.5$, and (c) $\lambda = 0.75$.

concentration phenomenon between the loading area and the nonloading area, the crack extension under asymmetric loading mode has strong directionality, the crack sprouting and the mutual penetration is more rapid, and along with the nonuniform rapid crack initiation and mutual penetration of the cracks, the acoustic emission ringing count rate shows a multipeak phenomenon.

3.3. Effect of the Degree of Load Asymmetry on the Regional Characterization of Damage. The evolution of the number of microcracks in the specimen with axial strain for different asymmetric coefficients is given in Figures 8 and 9 showing the crack distribution characteristics on the specimen surface at different loading moments (microscopic tensile cracks in black and microscopic shear cracks in blue). As can be seen from Figures 8 and 9, the number of cracks in the specimen

increases gradually with the increase of strain, and the crack number evolution curve has good correspondence with the stress−strain curve. According to the evolution process of crack number and strain, the specimen mesoscopic change process can be divided into four stages, i.e., calm period, crack initiation and stable expansion stage, unstable crack development and penetration stage, and postdestruction stage.

From Figures 8a and 9a, it can be seen that when $\lambda = 0$, the loading to point a (stress value 26.7 MPa, strain value 1.45%), the cracks start to initiate, and the cracks are sporadically distributed in the middle and end positions of the specimen. At point b (stress value of 34.5 MPa and strain value of 1.87%), the specimen is in the stage of steady crack expansion, and the total number of cracks in the specimen is 72. As the specimens were subjected to symmetrical homogeneous loading and the

specimens were precompressed, the cracks were distributed in a more symmetrical location, mainly in the region near the formation of the X-cracks. Point c (stress value 39.7%, strain value 2.19%) is at the junction of the stable crack extension stage and the unstable development stage, and the cracks are locally pooled at the positions of c1 and c2 at both ends of the specimen, approaching the state of local penetration. Point d (stress = 41.9 MPa, strain = 2.28%) is in the unstable expansion stage of the crack, and the crack penetration at c2 causes a rapid increase in the number of cracks. Point e (stress 43.6 MPa, strain 2.39%) is the peak moment, and the finely observed cracks are close to penetration in the X-shaped region. Point f (stress 40.9 MPa, strain 2.44%) is the postdamage state, where macroscopic damage is formed in the X-shaped region, and the number of cracks gradually increases due to the gradual increase in the degree of damage.

From Figures 8b and 9b, it can be seen that when $\lambda = 0.25$, after crack initiation at the moment of a (stress 7.26 MPa, strain 1.11%), the crack gradually expands downward along the direction parallel to the loading direction. Most of the cracks are in the interface region between the loaded and unloaded areas; a small number of cracks also exist in the middle of the loaded area; and eventually the dense cracks in the interface region and the cracks in the loaded area form through rupture surface, and the specimen undergoes macroscopic shear damage. From Figures 8c and 9c, it can be seen that when $\lambda = 0.50$, with the increase of strain value, the cracks first gather at the end of the upper loading plate and extend downward to the middle region of the specimen along the loading direction, then the cracks extend to the direction of the loading region to deflect, and finally form macroscopic shear rupture. Among them, point a (stress 14.96 MPa, strain 1.14%) is the moment of crack initiation, and the crack first appeared in the interface region between the loaded and unloaded zones. Point b is in the (stress 21.57, strain 1.55%) steady growth stage of displacement cracks, where the cracks are widely distributed between the loading region and the interface region and the number of cracks in the interface region is more than the number of cracks in the loading region. Points $c-e$ are the stages of crack instability development and penetration, in which the number of cracks increases rapidly with the increase of strain value and is concentrated in the interface region. After peak point e, a large number of cracks continue to be generated in the interfacing region and loading region on the shear rupture surface. From Figures 8d and 9d, it can be seen that when $a = 0.50$, point a (stress 19.2 MPa strain 1.13%) is the crack initiation moment, and the initial crack in the specimen appeared at the junction of the loaded and unloaded zones, close to the upper loaded plate. Point b is located in the stable crack expansion stage, and the number of cracks increases gradually with the increase of strain; there are nascent cracks in both the loading area and the interface area, and the number of cracks in the interface area is more than that in the loading area. Points $c-e$ show the crack instability increase, and through the stage, the number of cracks in this stage continues to increase, and the rate of growth increases gradually; the interface region near the upper loading plate is a stress concentration area; the cracks are generated from here and gradually expand downward; and there is a tendency to deflect to the loading area and eventually form a macroshear rupture. Point f is in the postdamage stage, and after the peak strength, a large number of cracks are generated in the lower part of the interface region as the strain increases and extends downward in the loading direction to form a second penetrating crack.

From the above analysis, it can be seen that the macroscopic rupture results of coal rock obtained from numerical simulation are in good agreement with the indoor test results. In conventional uniaxial compression, mesocracks initiate, nucleate, and expand near the X-shaped shear zone, until they penetrate each other to form macroscopic shear damage. When asymmetric loading is applied, the stress concentration effect caused by the edge of the upper loading plate is where the macroscopic shear rupture begins, and the cracks gradually expand from top to bottom, concentrating in the vicinity of the intersection interface between the loading area and the nonloading area until the cracks in the middle and lower parts of the specimen and the loading area are interconnected to form a macroscopic damage zone. By comparing with the results of Wang et al.[25] (Figure 10), the location of the dominant crack obtained from numerical simulation under asymmetric loading roughly matches with the in-house surface crack observation results and the location of the localized zone of the maximum shear strain field of the numerical scattering spot. Comparison of Figures 5 and 10 shows that the macroscopic damage patterns of coal samples under conventional uniaxial compression (symmetrical load) and uniaxial compression with asymmetric loading are significantly different. Macroscopic shear cracks are generated in the coal samples under conventional uniaxial compression conditions, which run through the specimens in an X-shape. The main control crack during asymmetric loading is basically located between the loaded and unloaded areas, and the expansion direction is approximately parallel to the loading direction.

3.4. Damage Constitutive Model Considering the Effects of Asymmetric Loading. Rock strength is a random variable governed by a number of factors, such as its material properties, confining pressure, and test conditions, but has a statistical distribution and can be described by the Weibull distribution.[33,34] Defining the rock statistical damage variable D as the ratio of the number of microelements that have been destroyed to the total number of microelements, it can be derived that

$$D = 1 - \exp\left[-\left(\frac{F}{n}\right)^m\right] \tag{2}$$

where F is the microelement strength variable. m and n are the characteristic parameters of the Weibull distribution, where m is a shape parameter indicating the degree of homogeneity of the material and n is a scale parameter related to the strength of the microelement.

From the ontological relations of the theory of damage mechanics for continuous media, it can be obtained that[35]

$$\sigma = E\varepsilon \exp\left[-\left(\frac{F}{n}\right)^m\right] \tag{3}$$

Equation 3 is the statistical ontological model of coal rock damage under uniaxial compression without considering the effect of asymmetric loading, where σ is the axial stress, ε is the axial strain, and E is the elastic modulus.

In this paper, the Drucker−Prager criterion is used to characterize microelement strength F. It is obtained that[36]

$$F = E\varepsilon\left(\frac{1}{\sqrt{3}} - \alpha\right) \tag{4}$$

$$\alpha = \frac{\sin \varphi}{\sqrt{3(3 + \sin^2 \varphi)}} \tag{5}$$

where α is the material parameter, and φ is the angle of internal friction of the material.

The statistical parameters m and n can be obtained from the peak intensity point of the stress–strain curve obtained from the test.

$$m = -\frac{1}{\ln(\sigma_c/E\varepsilon_c)}, \qquad n = \frac{F_c}{(1/m)^{1/m}} \tag{6}$$

The m and n in the statistical damage eigenmodel reflect the characteristics of the distribution of microdefects within the material with a size effect. When subjected to asymmetric loads, the change in the loading area leads to different distribution characteristics of microdefects in the corresponding area, resulting in different values of the parameters m and n. The statistical damage ontology model of coal rock reflecting the effect of asymmetric loading can be established by considering the relationship between the values of the parameters m and n and the asymmetric coefficient λ. The model can be used to analyze the effect of asymmetric loading on the coal rock.

From eq 6, there are three basic rock characteristic parameters, E, σ_c, and ε_c, in the parametric equations of the statistical ontological model of rock damage under different asymmetric loading factors. The problem of determining the parameters of the statistical damage principal model under different asymmetric loading conditions can be solved if the relationship between the rock mechanics characteristic parameters E, σ_c, and ε and the asymmetric coefficients is determined. Introducing the equivalent function of rock mechanical parameters when asymmetric loading is applied, the law of rock mechanical parameters when asymmetric loading is applied with homogeneous loading is expressed as follows

$$\begin{cases} \sigma_{c(\lambda)} = f(\lambda)\sigma_{c(0)} \\ \varepsilon_{c(\lambda)} = g(\lambda)\varepsilon_{c(0)} \\ E_{(\lambda)} = h(\lambda)E_{(0)} \end{cases} \tag{7}$$

where $E_{(\lambda)}$, $\sigma_{c(\lambda)}$, and $\varepsilon_{c(\lambda)}$ are the mechanical parameters of the material under different asymmetric coefficient loading conditions. $E_{(0)}$, $\sigma_{c(0)}$, and $\varepsilon_{c(0)}$ is the mechanical parameters of the material when the uniform load is applied. $f(\lambda)$, $g(\lambda)$, and $h(\lambda)$ are equivalent functions that reflect the relationship between asymmetric and uniform loads. Therefore, the statistical damage ontology model of coal rock considering the effect of asymmetric loading can be expressed as follows

$$\sigma_{(\lambda)} = E_{(\lambda)}\varepsilon_{(\lambda)}\exp\left[-\left(\frac{F}{n_{(\lambda)}}\right)^{m_{(\lambda)}}\right] \tag{8}$$

$$F = E_{(\lambda)}\varepsilon_{(\lambda)}\left(\frac{1}{\sqrt{3}} - \alpha\right) \tag{9}$$

$$m_{(\lambda)} = -\frac{1}{\ln\left(\dfrac{\sigma_{c(\lambda)}}{E_{(\lambda)}\varepsilon_{c(\lambda)}}\right)} \tag{10}$$

$$n_{(\lambda)} = -\frac{F_{c(\lambda)}}{\left[\dfrac{1}{m_{(\lambda)}}\right]^{1/m_{(\lambda)}}} \tag{11}$$

$$F_{c(\lambda)} = E_{(\lambda)}\varepsilon_{c(\lambda)}\left(\frac{1}{\sqrt{3}} - \alpha\right) \tag{12}$$

Equation 8 is the established statistical damage constitutive model of coal rock considering the effect of asymmetric loading; the expressions of a, b, and c functions are determined by eq 7, and the values of parameters m and n can be obtained by associating eqs 9−12 to give the theoretical curves of the stress–strain relationship.

The established damage model is validated using experimental data, and the mechanical parameters of coal rock under different asymmetry coefficients are shown in Table 3.

Table 3. Mechanical Parameters of Coal and Rock under Different Asymmetric Coefficients

λ	0	0.25	0.50	0.75
σ_c	47.88	33.97	21.06	6.27
ε_c	0.04	0.04	0.03	0.02
E	1.15	1.08	0.80	0.52

The data in Table 3 were fitted using eq 7 to give the relationship between the mechanical parameters under different asymmetric conditions and uniform load conditions, as shown in eq 13.

$$\begin{cases} \sigma_{c(\lambda)} = (0.998 - 0.979\lambda)\sigma_{c(0)} \\ \varepsilon_{c(\lambda)} = (1 - 0.074\lambda - 0.266\lambda^2)\varepsilon_{c(0)} \\ E_{(\lambda)} = (1 - 0.839\lambda + 0.041\lambda^2)E_{(0)} \end{cases} \tag{13}$$

Combined with the values of conventional uniaxial compression mechanical parameters, the mechanical parameters of coal rock under different asymmetric coefficients can be calculated by using eq 13, which can be substituted into eqs 9−13 to obtain the values of the parameters m and n in the damage constitutive model under the corresponding conditions, and the theoretically calculated and experimental values of each parameter under different conditions are shown in Table 4. As can be seen from Table 4, with the increase of the asymmetric coefficient, the value of parameter m and the value of parameter n both decrease gradually; the relationship between the value of m and the asymmetric coefficient can be expressed by a quadratic function, and the relationship between the value of n and the asymmetric coefficient can be expressed by a linear function.

The statistical damage ontological model of coal rock considering the effect of asymmetric loading can be established by substituting eq 13 into eq 8. Using the established damage ontology model, considering the effect of asymmetric loading combined with the stress–strain relationship of coal rock under uniform load, both the stress–strain curves of coal rock under any asymmetric coefficient can be determined. The stress–strain curves under asymmetric loading of coal rock are simulated using the above method, and the results of the comparison between the theoretically predicted curves and the experimental curves are shown in Figure 11.

Table 4. Values of the Parameters m and n

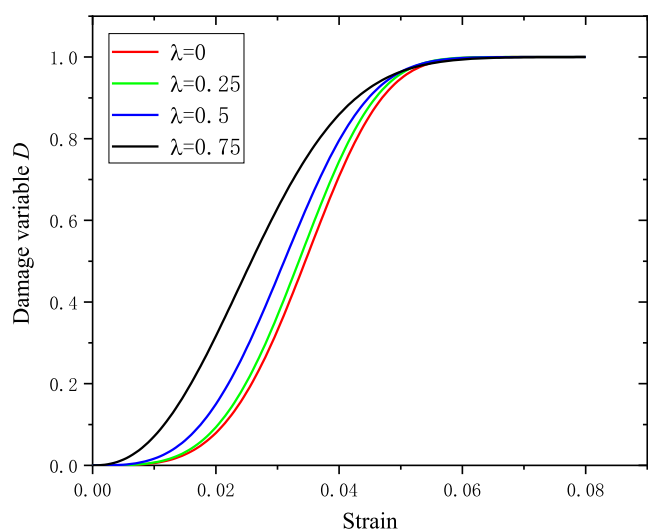| asymmetric coefficient λ	$\sigma_{c(\lambda)}$		$E_{(\lambda)}$		$\varepsilon_{(\lambda)}$		m	n
	experimental value	theoretical value	experimental value	theoretical value	experimental value	theoretical value		
0	43.31	43.24	2.06	2.07	0.027	0.027	3.92	32.79
0.25	32.55	32.64	1.68	1.64	0.026	0.026	3.71	25.23
0.5	22.01	22.04	1.19	1.23	0.025	0.024	3.38	17.61
0.75	11.50	11.45	0.83	0.82	0.021	0.021	2.34	10.42
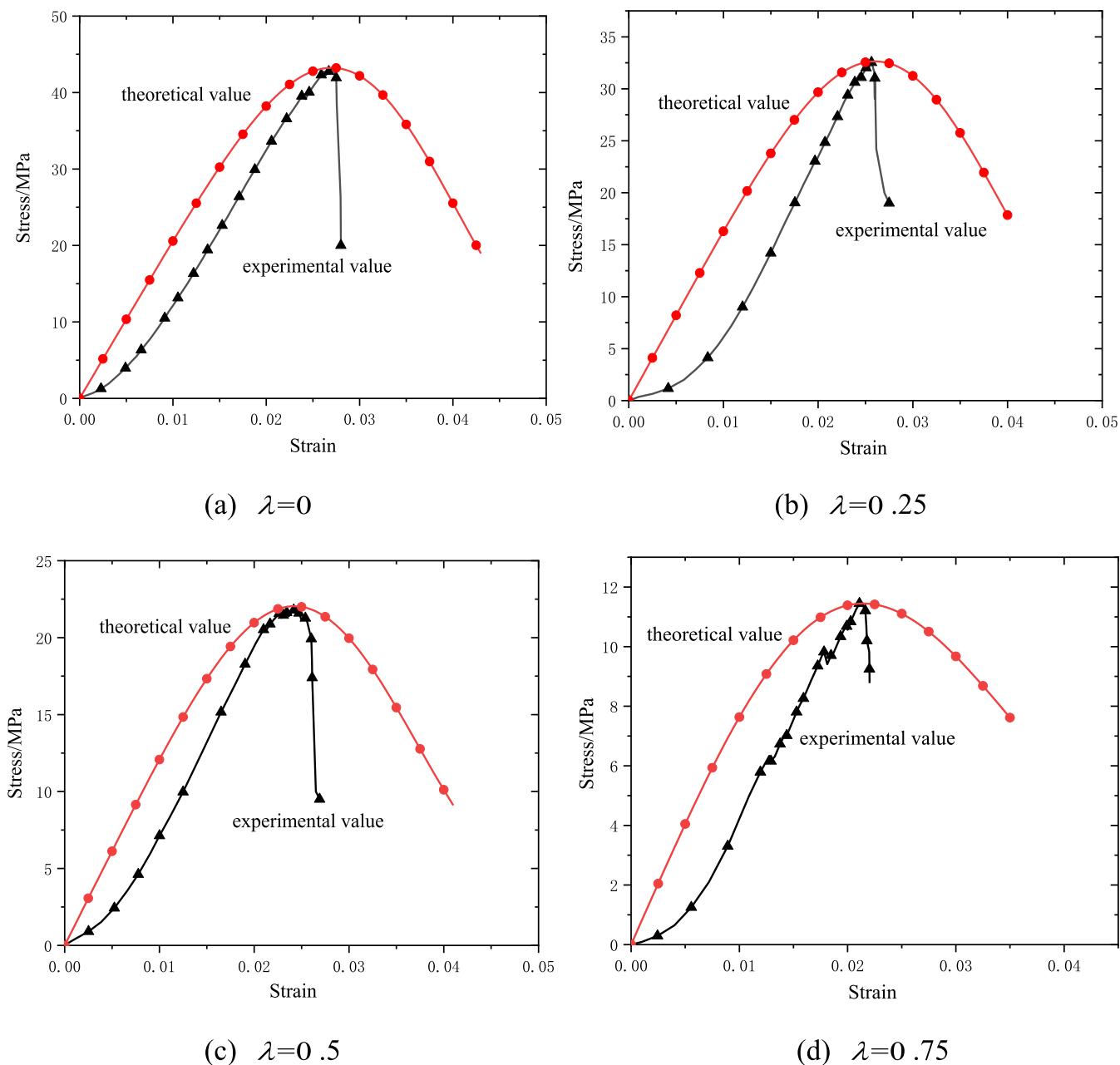
Figure 11. Comparison of theoretical model curve and experimental curves of coal under asymmetric load. (a) $\lambda = 0$ (b) $\lambda = 0.25$, (c) $\lambda = 0.5$, and (d) $\lambda = 0.75$.

As can be seen from Figure 11, the theoretical curves predicted by the statistical damage principal model established in this paper for coal rock under different asymmetric degrees of loading coincide well with the test curves, which indicates that the basic conception of the statistical principal model of coal rock damage, considering the asymmetric coefficient proposed in this paper is correct and reasonable. In the initial compression stage, the microscopic defects of coal rock are gradually closed and dense under compression, and the test curve is upward concave, and the slope of the tangent line at any point on the stress−strain curve in this stage is larger than the slope of the cut line at that point. The model developed in this paper does not consider the initial compaction stage of the coal rock, and the theoretical curve does not exhibit an up-concave shape. In the

elastic phase, the strain values in both the test curve and the theoretical curve increase gradually with the increase of the stress value, which is a linear function, and the theoretical curve is approximated as a straight line, reflecting the law that the elastic modulus of the coal rock is a certain value and is approximated to be parallel to the test curve; the theoretical curve is in good agreement with the test curve. In the plastic yielding stage, the slope of the test curve decreases gradually with the increase in the stress value, and the coal rock undergoes nonlinear deformation in this stage. The slope of the theoretical curve before the peak strength point decreases gradually with the increase of the uniaxial stress, reflecting an obvious plastic deformation stage, which is more consistent with the experimental results. The theoretical curve can better represent the stress—strain curve characteristics of this stage, especially in reflecting the peak stress and peak strain of coal rock. In the postpeak stage, the slope of the theoretical curve after the peak stress decreases gradually with the increase of the strain value, and the model curve shows the brittle ductile transition characteristic of the coal rock. The test curve shows a rapid drop of stress after reaching the peak stress, and the postpeak feature is not obvious, resulting in a slight difference between the theoretical curve and the test curve.

From the above analysis, it can be seen that the theoretical curve of the model agrees well with the test results under the condition of not considering the initial compaction stage. The damage statistical principal model developed in this article can better predict the stress—strain relationship of rocks with different asymmetry coefficients. In order to better verify the reasonableness of the statistical damage eigenmodel, based on the statistical method, the evolution relationship between damage variables and strain values under different asymmetric coefficients established is shown in Figure 12.

Figure 12. Damage factors that vary in their asymmetric coefficients with respect to strain.

As can be seen from Figure 12, the value of the damage variable D gradually increases to a stable value as the value of the axial strain increases. With the increase of asymmetric coefficient, the value of damage variable under the condition of the same strain value increases gradually, i.e., to reach the same value of damage variable, the larger the asymmetric coefficient is, the smaller the value of axial strain required is,

indicating that asymmetric loading plays a contributing role to the rock damage, and the stronger the asymmetricity is, the more prone the rock is to damage.

4. CONCLUSIONS

(1) The peak stress of the coal rock decreases gradually with the increase of the asymmetric coefficient of loading, and the two are linear functions of each other.

(2) The increase of acoustic emission parameters with strain value can be categorized into the initial compression-density stage, the elastic deformation stage, the crack initiation and stable extension stage, the unstable development and penetration of cracks stage, and the postdestruction stage. The peaks of the acoustic emission ringing counts are more concentrated during uniform loading and are mainly distributed in the unstable crack development and penetration stage and the postdamage stage. During asymmetric loading, the acoustic emission ringing count rate shows a multipeak phenomenon, and the peak points are more dispersed, which occurs in the stable crack extension stage and the unstable crack development and penetration stage.

(3) Under asymmetric loading, the location of the main control crack obtained by numerical simulation basically coincides with the indoor surface crack observation results and the location of the localized zone of the maximum shear strain field of the numerical scattering spot. When asymmetric loading is applied, the stress concentration effect caused by the edge of the upper loading plate is where the macroscopic shear rupture begins, and the cracks gradually expand from top to bottom, concentrating in the vicinity of the intersection interface between the loaded and unloaded zones.

(4) A statistical damage constitutive model considering the influence of asymmetric loads is established. The theoretical calculation results show that the larger the asymmetric coefficient is, the smaller the corresponding strain value is, which indicates that the asymmetric loads promote the damage of rock.

■ ASSOCIATED CONTENT

Data Availability Statement

All data, models, and code generated or used during the study appear in the submitted article.

■ AUTHOR INFORMATION

Corresponding Author

Xiangyang Zhang − *Key Laboratory of Safety and High-efficiency Coal Mining, Ministry of Education (Anhui University of Science and Technology), Huainan, Anhui 232001, China;* ⊙ orcid.org/0000-0002-1628-1770; Email: xyzhang_vip@126.com

Authors

Tao Wang − *School of Safety and Emergency Management Engineering, Taiyuan University of Technology, Taiyuan, Shanxi 030024, China; Key Laboratory of Safety and High-efficiency Coal Mining, Ministry of Education (Anhui University of Science and Technology), Huainan, Anhui 232001, China; Engineering Research Center of Phosphorus Resources Development and Utilization of Ministry of*

Education, Wuhan Institute of Technology, Wuhan, Hubei 430073, China

Hongbao Zhao − *School of Energy and Mining Engineering, China University of Mining and Technology (Beijing), Beijing 100083, China*

Wenpu Li − *School of Safety and Emergency Management Engineering, Taiyuan University of Technology, Taiyuan, Shanxi 030024, China*

Shuangli Du − *School of Safety and Emergency Management Engineering, Taiyuan University of Technology, Taiyuan, Shanxi 030024, China*

Complete contact information is available at:
https://pubs.acs.org/10.1021/acsomega.4c00720

Author Contributions

T.W.: conceptualization, investigation, writing—original draft. H.Z. and X.Z.: writing— review and editing, supervision. W.L. and S.D.: data curation, software, validation, visualization.

Notes

The authors declare no competing financial interest.
There are no ethical issues related to the research in this paper.

■ ACKNOWLEDGMENTS

■ REFERENCES

(1) Lu, S.; Bei, T.; Ma, Y.; Wang, H.; Sa, Z.; Liu, J.; Li, M.; Shi, J.; Wang, S. Strength Characteristics and Instability Mechanism of Combination of Intact Coal and Tectonic Coal Containing Gas Considering the Dip Angle of Interface. *Rock Mech. Rock Eng.* **2024**, *57*, 1395−1415.

(2) Wang, Z.; Li, J.; Lin, L.; Liu, B.; Ushakov, I. Mesoscopic Study on Instability Characteristics of Residual Coal Pillars-Roof System Based upon Domino Effect in Pillar Goaf. *Geomech. Geophys. Geo-Energy Geo-Resour.* **2023**, *9* (1), 109.

(3) He, B.-G.; Wang, L.; Feng, X.-T.; Zhen, R.-L. Failure Modes of Jointed Granite Subjected to Weak Dynamic Disturbance Under True-Triaxial Compression. *Rock Mech. Rock Eng.* **2023**, *56* (11), 7939−7957.

(4) Zhu, W.; Wang, F.; Chen, S.; Yin, D.; Zhou, J.; Jie, Z.; Zou, Y. Asymmetric Deformation Mechanism of Roadway with Continuous Mining and Continuous Backfilling. *Rock Mech. Rock Eng.* **2023**, 1−18.

(5) Jiang, Z.; Chen, D.; Xie, S. A Novel Asymmetric Stress Unloading Technology in Two Sides of Coal Roadway in Deep Mine: A Case Study. *Tunn. Undergr. Space Technol.* **2023**, *142*, 105452.

(6) Zhao, Y.; Song, H.; Liu, S.; Zhang, C.; Dou, L.; Cao, A. Mechanical Anisotropy of Coal with Considerations of Realistic Microstructures and External Loading Directions. *Int. J. Rock Mech. Min. Sci.* **2019**, *116*, 111−121.

(7) Xin, C.; Wang, K.; Du, F.; Zhang, X.; Wang, G.; Liu, Y. Mechanical Properties and Permeability Evolution of Gas-Bearing Coal under Phased Variable Speed Loading and Unloading. *Arabian J. Geosci.* **2018**, *11* (23), 747.

(8) Liu, Q.; Cheng, Y.; Jin, K.; Tu, Q.; Zhao, W.; Zhang, R. Effect of Confining Pressure Unloading on Strength Reduction of Soft Coal in Borehole Stability Analysis. *Environ. Earth Sci.* **2017**, *76* (4), 173.

(9) Ding, Z. W.; Jia, J. D.; Tang, Q. B.; Li, X. F. Mechanical Properties and Energy Damage Evolution Characteristics of Coal Under Cyclic Loading and Unloading. *Rock Mech. Rock Eng.* **2022**, *55* (8), 4765−4781.

(10) Gao, M.; Xie, J.; Gao, Y.; Wang, W.; Li, C.; Yang, B.; Liu, J.; Xie, H. Mechanical Behavior of Coal under Different Mining Rates: A Case Study from Laboratory Experiments to Field Testing. *Int. J. Min. Sci. Technol.* **2021**, *31* (5), 825−841.

(11) Zhang, Q.; Li, X.; Gao, J.; Jia, S.; Ye, X. Macro- and Meso-Damage Evolution Characteristics of Coal Using Acoustic Emission and Keuence Testing Technique. *Nat. Resour. Res.* **2022**, *31* (1), 517−534.

(12) Shan, T.; Li, Z.; Zhang, X.; Niu, Y.; Tian, H.; Zhang, Q.; Zang, Z.; Gu, Z.; Cai, C.; Liu, C. Infrared Radiation and Acoustic Emission of Damage Evolution and Failure Precursory for Water-Bearing Coal. *Rock Mech. Rock Eng.* **2022**, *55* (12), 7657−7674.

(13) Cui, B.; Feng, G.; Bai, J.; Wang, K.; Shi, X.; Wu, H. Acoustic Emission Characteristics and Damage Evolution Process of Backfilling Body-Coal Pillar-Backfilling Body Composite Structure. *Bull. Eng. Geol. Environ.* **2022**, *81* (8), 300.

(14) Gu, X.; Gong, X.; Zhang, C. G.; Gu, Y.; Wang, C.; Wang, G.; Guo, W. Drilled-Hole Number Effects on Energy and Acoustic Emission Characteristics of Brittle Coal. *J. Mater. Res. Technol.* **2023**, *23*, 3892−3903.

(15) Vallejos, J. A.; Salinas, J. M.; Delonca, A.; Mas Ivars, D. Calibration and Verification of Two Bonded-Particle Models for Simulation of Intact Rock Behavior. *Int. J. Geomech.* **2017**, *17* (4), 06016030.

(16) Liu, W.; Yuan, W.; Yan, Y.; Wang, X. Analysis of Acoustic Emission Characteristics and Damage Constitutive Model of Coal-Rock Combined Body Based on Particle Flow Code. *Symmetry* **2019**, *11* (8), 1040.

(17) Wu, N.; Liang, Z.; Zhou, J.; Zhang, L. Energy Evolution Characteristics of Coal Specimens with Preformed Holes under Uniaxial Compression. *Geomech. Eng.* **2020**, *20* (1), 55−66.

(18) Liu, T.; Lin, B.; Zou, Q.; Zhu, C.; Guo, C.; Li, J. Investigation on Mechanical Properties and Damage Evolution of Coal after Hydraulic Slotting. *J. Nat. Gas Sci. Eng.* **2015**, *24*, 489−499.

(19) Sun, C.; Cao, S.; Li, Y. Mesomechanics Coal Experiment and an Elastic-Brittle Damage Model Based on Texture Features. *Int. J. Min. Sci. Technol.* **2018**, *28* (4), 639−647.

(20) Huang, P.; Zhang, J.; Damascene, N. J.; Dong, C.; Wang, Z. A Fractional Order Viscoelastic-Plastic Creep Model for Coal Sample Considering Initial Damage Accumulation. *Alexandria Eng. J.* **2021**, *60* (4), 3921−3930.

(21) Xu, Q.; Yao, Q.; Yu, L.; Zhu, L.; Chong, Z.; Li, Y.; Li, X. Mechanical Properties and Damage Constitutive Model of Coal Specimen with Different Moisture under Uniaxial Loading. *Int. J. Damage Mech.* **2023**, *32* (3), 462−481.

(22) Zang, A.; Christian Wagner, F.; Stanchits, S.; Dresen, G.; Andresen, R.; Haidekker, M. A. Source Analysis of Acoustic Emissions in Aue Granite Cores under Symmetric and Asymmetric Compressive Loads. *Geophys. J. Int.* **1998**, *135* (3), 1113−1130.

(23) Yoon, J. S.; Zang, A.; Stephansson, O. Simulating Fracture and Friction of Aue Granite under Confined Asymmetric Compressive Test Using Clumped Particle Model. *Int. J. Rock Mech. Min. Sci.* **2012**, *49*, 68−83.

(24) Wang, X.; Wen, Z.; Jiang, Y.; Huang, H. Experimental Study on Mechanical and Acoustic Emission Characteristics of Rock-Like Material Under Non-Uniformly Distributed Loads. *Rock Mech. Rock Eng.* **2018**, *51* (3), 729−745.

(25) Wang, T.; Zhao, H.; Ge, L.; Zhang, H.; Liu, R. Study on Deformation Evolution Law of Coal under Asymmetric Loading by Digital Image Correlation. *Appl. Opt.* **2020**, *59* (34), 10959−10966.

(26) Wang, Z.; Li, F.; Mei, G. OpenMP Parallel Finite-Discrete Element Method for Modeling Excavation Support with Rockbolt and Grouting. *Rock Mech. Rock Eng.* **2024**, 03746.

(27) Wei, J.; Wang, S.; Song, S.; Sun, Q.; Yang, T. Experiment and Numerical Simulation of Overburden and Surface Damage Law in Shallow Coal Seam Mining under the Gully. *Bull. Eng. Geol. Environ.* **2022**, *81* (5), 207.

(28) Liu, X.; Chen, H.; Liu, B.; Deng, W.; Liu, Q.; Zhang, Z. Experimental and Numerical Study on Failure Characteristics and Mechanism of Coal under Different Quasi-Static Loading Rates. *Theor. Appl. Fract. Mech.* **2022**, *121*, 103478.

(29) Deng, Q.; Liu, J.; Wang, J.; Lyu, X. Mechanical and Microcrack Evolution Characteristics of Roof Rock of Coal Seam with Different Angle of Defects Based on Particle Flow Code. *Materials* **2023**, *16* (4), 1401.

(30) Kong, B.; Zhuang, Z.; Zhang, X.; Jia, S.; Lu, W.; Zhang, X.; Zhang, W. A Study on Fractal Characteristics of Acoustic Emission under Multiple Heating and Loading Damage Conditions. *J. Appl. Geophys.* **2022**, *197*, 104532.

(31) Wen, Z.; Jiang, P.; Song, Z.; Jiang, Y.; Wen, J. Study on Damage Characteristics and Application of Gypsum Pillar Strengthened with FRP. *Geomech. Geophys. Geo-Energy Geo-Resour.* **2024**, *10* (1), 13.

(32) Zang, Z.; Li, Z.; Niu, Y.; Yin, S. Experimental Investigation of the Fracture and Damage Evolution Characteristics of Flawed Coal Based on Electric Potential and Acoustic Emission Parameter Analyses. *Eng. Fract. Mech.* **2024**, *295*, 109740.

(33) Wu, L.; Wang, Z.; Ma, D.; Zhang, J.; Wu, G.; Wen, S.; Zha, M.; Wu, L. A Continuous Damage Statistical Constitutive Model for Sandstone and Mudstone Based on Triaxial Compression Tests. *Rock Mech. Rock Eng.* **2022**, *55* (8), 4963−4978.

(34) Ali, M.; Wang, E.; Li, Z.; Wang, X.; Khan, N. M.; Zang, Z.; Alarifi, S. S.; Fissha, Y. Analytical Damage Model for Predicting Coal Failure Stresses by Utilizing Acoustic Emission. *Sustainability* **2023**, *15* (2), 1236.

(35) Li, X.; Cao, W.-G.; Su, Y.-H. A Statistical Damage Constitutive Model for Softening Behavior of Rocks. *Eng. Geol.* **2012**, *143−144*, 1−17.

(36) Fang, W.; Jiang, N.; Luo, X. Establishment of Damage Statistical Constitutive Model of Loaded Rock and Method for Determining Its Parameters under Freeze-Thaw Condition. *Cold Reg. Sci. Technol.* **2019**, *160*, 31−38.